Seismic performance of diagonally braced cold-formed thin-walled steel composite walls

XU Yunpeng[1]，ZHANG Haibin[2]，XIA Xiang[3]，LIU Yuqing[4]，YANG Xiuhong[4]，GONG Dazhuang[4]

(1. School of Civil Engineering；Key Laboratory of New Technology for Construction of Cities in Mountain Area，Ministry of Education，Chongqing University，Chongqing 400045，P. R. China；2. Shandong Laigang Constuction Co. Ltd，Qingdao 266000，Shandong，P. R. China；3. Management Committee of Dafosi Scenic Area，Chongqing 402660，P. R. China；4. BNBM House Co. Ltd，Beijing 100070，P. R. China)

Abstract：Through an experimental investigation of the seismic performance of diagonally braced cold-formed thin-walled steel composite walls subjected to vertical loads，the mechanical properties，failure modes，and hysteresis properties of the walls were elucidated. In addition，the influence of a sheathing panel on the hysteresis performance，ductility，and energy dissipation of the composite walls was analyzed. The experimental results show that the shear bearing capacity of the single-sided oriented strand board (OSB) panel wall was increased by 38. 79% compared with the non-panel wall under the same vertical load. The shear bearing capacity，ductility coefficient，μ，and energy dissipation factor，E，of the single-sided OSB panel composite wall with an axial compression ratio of 0. 24 were increased by 7. 5%，4. 5%，and 4. 1%，respectively，compared to the wall with an axial compression ratio of 0. 16；however，the yield displacement was reduced by 8. 1%. The cold-formed thin-walled steel composite wall with diagonal bracing exhibited good seismic performance. After verifying the reliability of the finite element model，the influence of the axial compression ratio of the wall stud and the yield strength of the steel components on the mechanical performance of the wall was investigated through a variable parameter analysis. The results showed that with the increasing axial compression ratio，the shear bearing capacity of the wall was improved. In addition，reducing the yield strength of the steel components significantly reduced the shear capacity of the composite wall. Finally，according to the *Technical Specification for Low-rise Cold-formed Thin-walled Steel Buildings* (JGJ 227-2011) and AISI S400-15，the resistance partial coefficient of the wall was derived，which determines the design value for the shear bearing capacity under a horizontal earthquake.

Keywords：cold-formed thin-walled steel；composite wall；diagonal support；seismic performance；experimental research；finite element analysis

加斜撑冷弯薄壁型钢组合墙体的抗震性能

徐云鹏[1],张海宾[2],夏祥[3],刘宇清[4],杨秀红[4],宫大壮[4]

(1. 重庆大学 土木工程学院；山地城镇建设与新技术教育部重点实验室,重庆 400045;2. 山东莱钢建设有限公司,山东 青岛 266000;3. 大佛寺风景区管委会, 重庆 402660;4. 北新房屋有限公司,北京 100070)

摘　要：通过对竖向荷载作用下加斜撑冷弯薄壁型钢组合墙体的抗震性能试验研究,考察了墙体的受力特性、破坏模式和滞回性能,分析了覆面板对组合墙体滞回性能、延性和耗能能力的影响。结果表明:相同竖向荷载作用下,单面覆 OSB 板墙体较无面板墙体的抗剪承载力提高了 38.79%;墙架柱轴压比为 0.24 较轴压比为 0.16 的单面覆 OSB 板组合墙体抗剪承载力提高了 7.5%,屈服位移降低了 8.1%,墙体延性系数 μ 提高了 4.5%,耗能系数 E 提高了 4.1%,加斜撑冷弯薄壁型钢组合墙体体现出较好的抗震性能。在对有限元模型可靠性进行验证的基础上,通过变参数分析考察了墙架柱轴压比、钢龙骨屈服强度对墙体受力性能的影响规律,结果表明:随墙架柱轴压比的增大,组合墙体的抗剪承载力有所提高;减小钢龙骨的屈服强度,组合墙体的抗剪承载力下降明显。依据《低层冷弯薄壁型钢房屋技术规程》(JGJ 227—2011)和美国规范 AISI S400-15,推导出墙体的抗力分项系数,确定了水平地震作用下此类墙体的抗剪承载力设计值。

关键词：冷弯薄壁型钢;组合墙体;斜向支撑;抗震性能;试验研究;有限元分析

1　Introduction

In recent years, green prefabricated buildings have been vigorously promoted in China, and cold-formed thin-walled steel structure residential systems have rapidly emerged as representative prefabricated building structures. The composite wall, which consists of a panel material and steel keel, is the main bearing member of cold-formed thin-walled steel structure residential systems.

Blum et al.[1] studied the bending support of cold-formed thin-walled steel walls. Through tests and analysis, design expressions for support stiffness and strength were proposed, and the concepts of minimum support stiffness and corresponding imperfections were introduced. Hikita et al.[2] carried out an investigation of the shear bearing capacity of a light steel frame shear wall subjected to an extra gravity load under monotonic and low-cycle reverse loads. The results showed that the existence of an additional gravity load had no obvious effect on the shear bearing capacity of a steel frame shear wall with a plate. Tian et al.[3] carried out a theoretical analysis of a cross flat steel-braced cold-formed steel frame wall. Based on the angle-displacement method, a first-order elastic analysis was used to predict the shear bearing capacity of the cross flat steel braced cold-formed steel frame wall. Gad et al.[4] studied the interaction between the components of a cold-formed steel composite wall and the shear bearing capacity of the whole wall. Horizontal low-cycle reverse loading tests were carried out on a cold-formed steel wall with cross-bracing and a panel, revealing that the yield strength of the x-cross bracing controlled the bearing capacity of the wall.

Liu[5] studied the hysteresis properties of a steel plate shear wall and an anti-buckling steel plate shear wall subjected to vertical loads. The results indicated that the shear bearing capacity and energy dissipation capacity of the steel plate shear wall and anti-buckling steel plate shear wall were reduced as a result of the vertical load, but the lateral stiffness of the anti-buckling steel plate shear wall was not affected by the vertical load. Hao et al.[6] studied the shear bearing capacity of a cross steel strip braced composite wall consisting of a cold-formed thin-walled steel frame and light weight mortar. A joint plate was added to the specimens to strengthen the screw connection between the brace and the steel skeleton in the experiments. The results showed that the shear bearing capacity of the composite wall was greatly improved by the joint plate. Dong[7] studied the shear bearing capacity of a cold-formed thin-walled composite wall with a sandwich steel plate. The results showed that the cross steel strip controlled the shear bearing capacity of the wall; reducing the screw spacing could improve the lateral stiffness and shear bearing capacity of the wall. Chen[8]

carried out an investigation of the shear bearing capacity of a cold-formed thin-walled composite wall with cross bracing. It was noted that the buckling of the side column of the cross-braced wall under monotonic loading was caused by the eccentric tension, while the damage to the wall under a low-cycle reverse load was due to the extrusion deformation of the lower guide beam. Wang et al.[9] studied the seismic behavior of cold-formed thin-walled walls with diagonal braces. The results showed that the arrangement of the diagonal bracings resulted in improvement of the load bearing capacity, stiffness and energy dissipation of the walls. However, the diagonal brace increased the lateral performance to a limited extent, because the connection between the diagonal brace and the transverse brace was weak and buckling of the transverse brace occurred early. The integrity of the wall panel has a significant influence on the lateral performance of the wall. Reducing the screw spacing around the wall panel can improve the bearing capacity, stiffness, and energy dissipation capacity of the wall markedly; however, the ductility will decrease.

Although there have been many experimental studies and theoretical analyses of the seismic performance of cold-formed thin-walled steel composite walls, studies on the mechanical behavior of cold-formed thin-walled steel composite walls are uncommon; systemic studies on the seismic performance of such walls under vertical loading are still lacking. In this study, an experimental investigation and theoretical analysis of a diagonally braced cold-formed thin-walled steel composite wall under vertical loading were carried out to investigate the mechanical properties, failure modes, and hysteresis properties of the wall. In addition, the influence of the axial compression ratio of the wall studs and the yield strength of the steel components on the seismic performance of the wall were also investigated. Based on the results of the experiments and finite element parameter analysis, a design method and suggestions for these walls in seismic design are proposed.

2   Wall Design

2. 1   Wall Structure

In these experiments, six full-sale cold-formed thin-walled steel composite walls with diagonal bracing were designed and divided into three groups based on the inclusion of a panel and the value of the vertical force, each group of walls was identical in material, size, and loading method. The configurations are detailed in Table 1. The first group of walls was placed under a vertical load of 80 kN without a panel. The second group was placed under a vertical load of 80 kN and included a single-sided oriented-strand board (OSB) panel. The third group was placed under a vertical load of 120 kN and included a single-sided OSB panel. The first and second groups were compared to analyze the effect of the panel on the shear bearing capacity of the wall. The second and third groups were compared to analyze the effect of different vertical loads (i. e. , the axial compression ratio of the wall stud) on the shear bearing capacity of the wall with a single-sided OSB panel. The wall numbers and test parameters are listed in Table 1.

The columns of the composite wall were composed of C-section cold-formed thin-walled steel member (C140 mm×40 mm×11 mm×1. 2 mm) spaced at 400 mm; the upper guide beam, lower guide beam, and diagonal bracing of the wall were composed of U-section cold-formed thin-walled steel member (U143 mm×40 mm×1. 2 mm). The columns on both sides of the wall and the middle column were composed of two C-shaped cold-formed thin-walled steel members and connected to the I-section by a double row of self-tapping screws. In addition, the side columns were covered by U-section cold-formed thin-walled steel members to avoid premature buckling, and the self-tapping screws were spaced at 100 mm. The diagonal bracing was composed of two C-section cold-formed thin-walled steel members, which were connected to the I-section by a double row of self-tapping screws.

The openings at the middle of the diagonal bracing were used to keep the column continuous. To strengthen the screw connection between the diagonal bracing and the column，the inter-section of the diagonal bracing and the column was strengthened locally by a 3-mm-thick gusset plate. The thickness of the OSB panel of the wall was 12 mm，and the size of a single panel was 2. 4 mm× 1. 2 mm（height × width）. On the inside and outside of the wall，self-tapping screws were spaced at intervals of 150 mm between the panel and the steel frame. The steel frames were assembled using ST4800 self-tapping screws，the OSB panel and the steel frame were assembled using ST4835 self-tapping screws，and the connection between the anti-drawing component and the steel frame was made with ST5330 self-tapping screws. The anti-drawing components at the four corners of the wall were connected to the upper guide beam and the lower guide beam by M16 bolts，while the upper guide beam and the upper guide were connected to the loading device with M12 bolts. Detailed dimensions of the wall are depicted in Fig. 1.

Table 1   Wall number and test parameters

Number	Grouping	Wall number	Wall parameters （$H \times b$）	Panel	Bracing form	Loading	
						Loading mode	Vertical force /kN
1	First group	A1－1		without			80
2	Wall A1	A1－2					
3	Second group	A2－1	2. 4 m×2. 4 m	with	V-shape	Low-cycle reverse loading	80
4	Wall A2	A2－2	column spacing				
5	Third group	A3－1	400 mm	with			120
6	Wall A3	A3－2					

2. 2   Material properties

The material properties of the Q345 steel and the OSB panel were measured as set out in standard GB/T228. 1-2010[10] by making plate specimens. The measurement results for the Q345 steel and the material properties of the OSB panel are listed in Tables 2 and 3，respectively.

Table 2   Material property test results of steel

Number	Nominal dimension	Yield strength /（N・mm^{-2}）		Tensile strength/ （N・mm^{-2}）		Elongation/%		Elasticity modulus/MPa	
		Test value	Average	Test value	Average	Test value	Average	Test value	Average
S－1		363		469		45		175 491	
S－2	200 mm×10 mm× 1. 2 mm	360	358	464	462	44	44. 4	173 507	178 820. 37
S－3		350		454		44		187 462	

Table 3   Physical properties of 12-mm-thick OSB panel

Index	Unit	12 mm-thick OSB plate
Static bending strength［parallel/vertical］	MPa	22/11 or 22/7. 86
Bending elasticity modulus［parallel/vertical］	MPa	3 500/1 400
Internal bond strength	MPa	X_{max}：0. 79；X_{min}：0. 53
24 h Water absorption and thickness swelling	%	X_{min}：7. 1；X_{max}：8. 9
Deviation of board density	%	±10
Moisture content	%	5. 7
Formal dehyde emission E1 stage［E2 stage］	mg/L	0. 02

(a) Dimension of wall A1

(b) Dimension of wall A2&A3
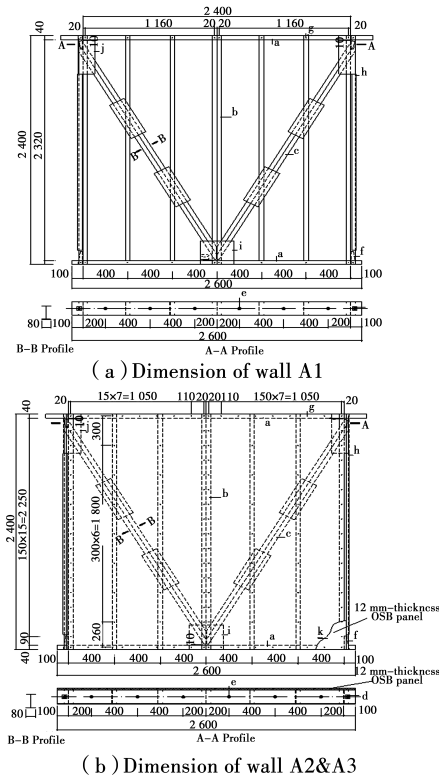
Fig. 1   Dimension of walls(mm)

2.3   Loading device and testing procedure

The test loading device is shown in Fig. 2. At the four corners of the top and bottom of the wall, the wall and the top and bottom beams of the loading device were connected with M16 bolts, in which 150 mm× 150 mm× 20 mm (length × width × thickness) rectangular cushion blocks were arranged, to allow the vertical load to be accurately transferred to each wall stud. In addition, the wall was fastened to the slots in the top and bottom beams of the loading device by M12 bolts spaced at a distance of 400 mm. The horizontal actuator was connected to the web of the top guide beam through the top loading beam. On the lateral side of the top loading beam, sliding bracings were arranged to provide a lateral restraint force and prevent loss of out-of-plane stability.

In accordance with the requirements for shear tests of cold-formed thin-walled steel walls set out in standard JGJ 227-2011[11], the measurement points were arranged as shown in Fig. 3. Eight displacement sensors were arranged to measure the displacements of the wall specimens and the loading
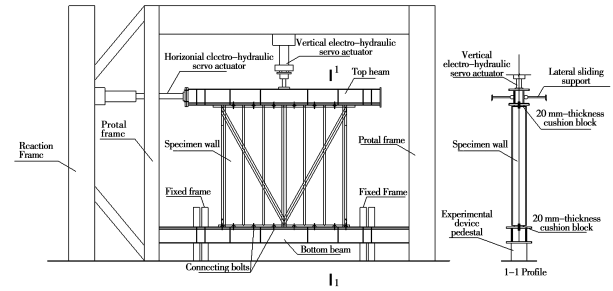
Fig. 2   Test loading device

device (Fig. 3). Sensor D1 was used to measure the displacement of the horizontal actuator connected to the top beam, sensor D2 measured the horizontal relative displacement between the wall specimen and the top loading beam, and sensors D3 and D4 measured the relative slipping displacements between the wall and the bottom loading beam. Sensors D5 and D6 were used to measure the vertical relative displacement between the wall and the bottom loading beam; sensors D7 and D8 measured the vertical relative displacement between the bottom loading beam and the ground. In Fig. 3, "A" represents the vertical distance from sensor D2 to the bottom surface of the top loading beam, which was set as 600 mm; "B" and "C" represent the horizontal distances from sensors D5 and D6 to the lateral surface of the side column of the wall, which were set as 100 mm.
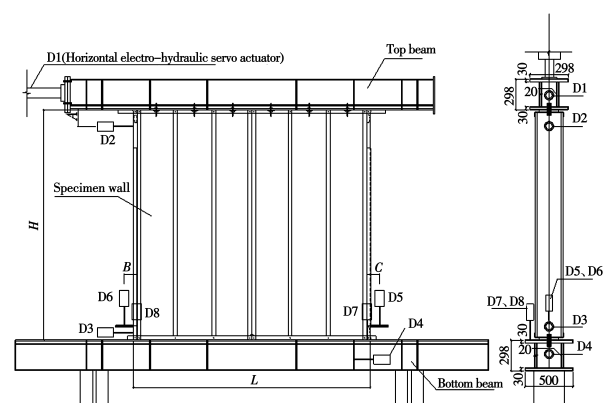
Fig. 3   Displacement meter arrangement(mm)

2.4   Loading process

The previous finite element simulation predicted a yield displacement of the wall of 12 mm. The tests were conducted using the displacement control method under a horizontal low-cycle reverse load. A preload

was applied at a rate of 0．4 mm/s with a displacement increment per stage of 0．125 Δ_y until 3 mm and cycled once． Then，the formal loading stage was applied，with a displacement increment per stage of 4 mm until 12 mm（yield displacement），and cycled once per stage． After yielding，the wall was loaded with a displacement increment per stage of 0．5 Δ_y and cycled three times until the wall was destroyed．

In these tests，the vertical force was loaded to the specified value once through the vertical actuator． The vertical force was initially kept constant and readings from all sensors were recorded simultaneously． The vertical force was applied using the load-control method at a rate of 0．2 kN/s． During the horizontal loading process，the displacement data for each sensor and the actuator load were collected and recorded by a ZI-160 data collection instrument．

3   Test results and analysis

3.1   Test observations

3.1.1   Wall A1

For wall A1，the experimental phenomenon was basically the same，so only wall A1-1 is described． Owing to the low in-plane stiffness of the wall without a panel，the force increased slowly with increasing horizontal displacement；thus the change was not obvious in the early stage of the test． When the horizontal displacement reached 12 mm，obvious wrinkles appeared in the flange of the diagonal bracing close to the upper guide beam，and the thrust of the horizontal actuator reached 24．03 kN． With further increase in the horizontal displacement，the wrinkles in the left and right diagonal bracings occurring at the area of the gusset plate became more obvious． When the horizontal displacement reached 18 mm，the local buckling of the diagonal bracing subjected to pressure was obvious，and the deformation was larger，as shown in Fig. 4（a）．

When the horizontal displacement reached 24 mm，the self-tapping screws of the gusset plate in

（a）Local buckling of diagonal bracing （b）Shear fracture of screws at gusset plate

（c）Severe damage of screws at gusset plate （d）Snap of diagonal bracing
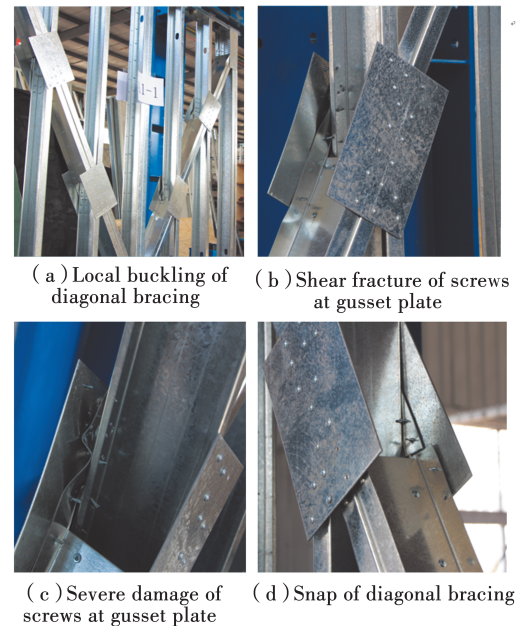
Fig. 4   Failure of wall A1-1

the middle bottom of the wall exhibited sliding and then shear failure as the test was carried out． At the inter-section with the middle gusset plate，the diagonal bracing exhibited severe bending，and some of the self-tapping screws were torn out，as shown in Fig. 4（b）and（c）． Meanwhile，the gusset plate and the wall frame connection exhibited obvious dislocation． As the horizontal displacement continued to increase，the deformation of the wall also continued to increase，but the load began to decrease． When the horizontal displacement reached 42 mm，the left bracing was pulled to breaking，as shown in Fig. 4（d）． With increasing horizontal displacement，the deformation of the wall was accelerated，and the load decreased． When the load reached 85％ of the ultimate load，the test was stopped．

3.1.2   Wall A2

For wall A2，the experimental phenomenon was basically the same，so only wall A2-1 is described． Owing to the effect of the OSB panel on the lateral stiffness of the wall，the force increased rapidly with increasing horizontal displacement． At the elastic stage of the wall，the flange of the diagonal bracing close to the upper and lower guide beam exhibited obvious wrinkles in the tension and

compression process, as shown in Fig. 5(a). When the horizontal displacement reached 18 mm, the bending of the left and right diagonal bracing at the gusset plate became more obvious, and the screws connecting the OSB panel to the steel skeleton at the corners became cut into the panel, as shown in Fig. 5 (b). When the horizontal displacement reached 30 mm, the bearing capacity reached 50. 12 kN. The compression diagonal bracing at the gusset plate in the middle bottom of the wall exhibited intense bending, while the lower guide beam and the stud exhibited different levels of buckling, as shown in Fig. 5(c). At the joint area on the back of the OSB panel, the screws became embedded into the panel, causing minor shedding of the OSB panel, as shown in Fig. 5(d). When the horizontal displacement reached 36 mm, the screws on the gusset plate at the intersection of the V-shaped diagonal bracing were torn out, the diagonal bracing and upper and lower guide beams were severely deformed, and sliding occurred between the gusset plate and the guide beam, as shown in Fig. 5(e).

When the horizontal displacement reached 48 mm, the screws connecting the middle gusset plate and the lower guide beam were torn out, the joint area was severely deformed, and the screws at the bottom corner on the back of the OSB panel were torn out. This resulted in different levels of shedding of the OSB panel, as shown in Fig. 5(f). With increasing horizontal displacement, the deformation of the wall accelerated and the load decreased. When the load reached 85% of the ultimate load, the test was stopped. The global failure mode is shown in Fig. 5(g).

3. 1. 3　Wall A3

For wall A3, the experimental phenomenon was basically the same, so only wall A3-2 is described. In the elastic stage, the test behavior of wall A3-1 and A3-2 was similar to that of wall A2-1 and A2-2. In the reverse loading process, the flange of the diagonal bracing subjected to pressure at the gusset

(a) Yield of flange of diagonal bracing　(b) Shear fracture of screws at gusset plae

(c) Yield of lower guide beam and studs　(d) Shedding of the OSB panel at joint area

(e) Slipping of the gusset plate　(f) Shedding of the OSB panel at corners

(g) Global failure mode
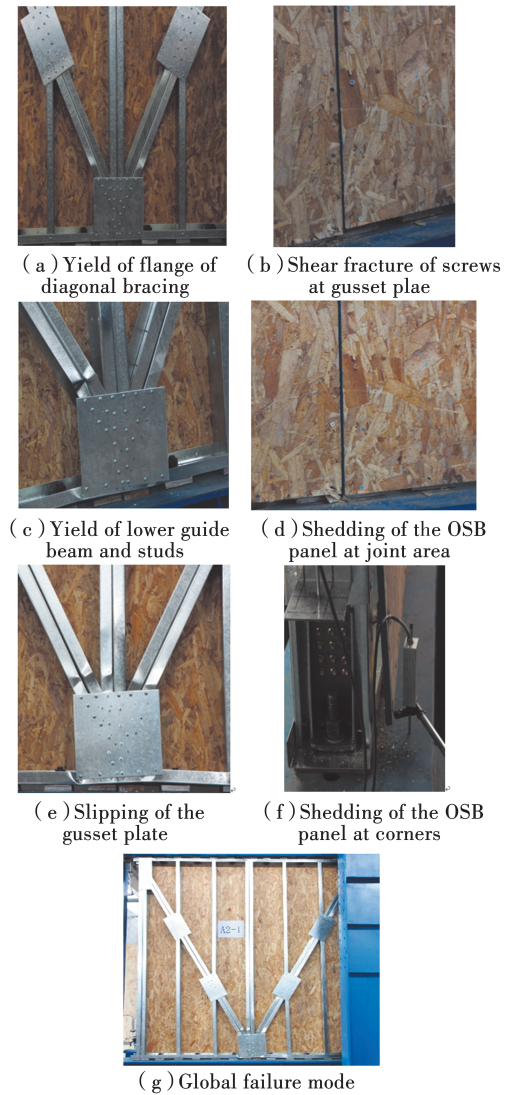
Fig. 5　Failure of wall A2-1

plate exhibited obvious local buckling, as shown in Fig. 6 (a). When the horizontal displacement reached 12 mm, the screws in the bottom corner of the OSB panel became embedded into the panel, the wrinkles of the compressive diagonal bracing at the gusset plate became more obvious, and a noticeable relative angle occurred between the gusset plate and lower guide beam, as shown in Fig. 6 (b). When the horizontal displacement increased from 12 mm to 18 mm, the upper parts of the left and right studs exhibited obvious buckling; the deformation of the flange and crimping of the studs is shown in Fig. 6(c). With further increase in the horizontal displacement, the force applied to the wall increased. When the displacement reached 24 mm, the bearing capacity reached 55. 99 kN.

The buckling of the middle stud near the lower guide beam at this point is shown in Fig. 6(d). As the horizontal displacement continued to increase, the bearing capacity began to decrease, and the screws in the middle part of the gusset plate were torn out, as shown in Fig. 6(e).

At the joint area on the bottom of the OSB panel, the screws were cut into the panel and caused minor shedding of the panel. As the horizontal displacement continued to increase, the screws connecting the lower guide beam and the middle part of the gusset plate were torn out, and the diagonal bracing subjected to pressure became severely wrinkled and deformed. When the horizontal displacement reached 48 mm, the bearing capacity decreased to 39. 62 kN. Meanwhile, the screws connecting the panel and the steel skeleton were cut into the panel, and different degrees of separation occurred between the corner of the panel and the steel skeleton, as shown in Fig. 6 (f). With increasing horizontal displacement, the deformation of the wall accelerated and the load decreased. When the load reached 85% of the ultimate load, the test was stopped. The global failure mode is shown in Fig. 6(g).

The observed test behaviors reveal that without the constraint from the panel, the shear bearing capacity of wall A1 was small, but the lateral stiffness of the wall was improved owing to the effect of the V-shaped diagonal bracing and the gusset plate. Most of the damage occurred in the area of the gusset plate, and the shear fracture of the screws and breaking of the diagonal bracing represented failure of the wall. Compared with wall A1, the lateral stiffness and shear bearing capacity of wall A2 were improved by the constraint from the panel. The shear failure of the screws in the gusset plate and panel represented failure of the wall. Comparing wall A3 with wall A2, as a result of the increased vertical load, the side studs of wall A3 exhibited buckling earlier, but both wall A3 and A2 were destroyed when the screws on the gusset plate and panel underwent shear fracture and the middle studs and guide beams yielded.

(a) Yield of flange of   (b) Rotation of the
    diagonal bracing   gusset plate

(c) Yield of the side stud   (d) Yield of the middle stud

(e) Shear fracture of screws   (f) Shear fracture of OSB
    at gusset plate   panel in bottom

(g) Global failure mode
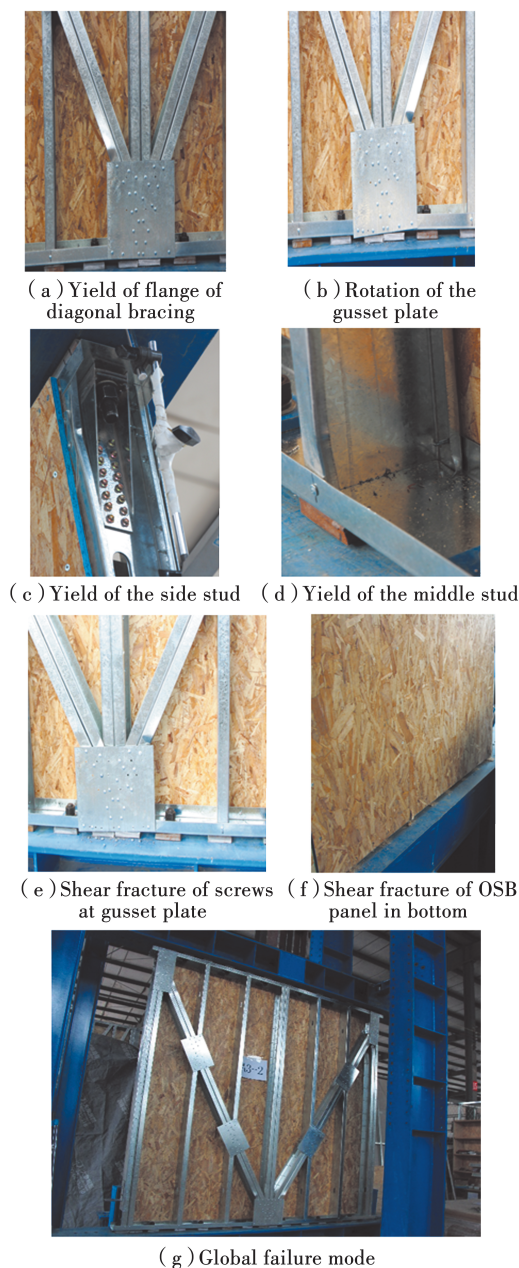
Fig. 6   Failure of wall A3-2

3. 2   Test data processing

The whole lateral displacement, δ_0, at the top of the wall measured during the tests consists of three parts: δ_φ is the lateral displacement of the top of the wall when the wall undergoes rotation caused by the extension of the anchor bolts, δ_1 is the relative sliding displacement between the wall and the pedestal, and δ is the actual shear deformation of the wall (Fig. 7).

Thus, the actual lateral displacement at the top of the wall, which is the shear deformation (Δ), can be expressed with Eq. (1).
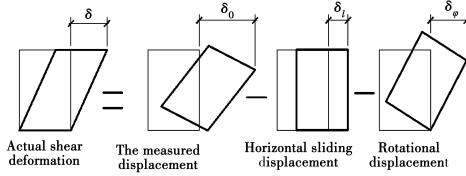
Fig. 7 Shear-displacement model of composite walls

$$\Delta = \delta = \delta_0 - \delta_l - \delta_\varphi \qquad (1)$$

where δ_0 is the actual data measured by sensor $D2$ considering the height reduction. It is defined as the actual lateral displacement of the top of the wall: $\delta_0 = \frac{1}{2}\left(\frac{HD_2}{H-600}+D_1\right)$, where D_1 is the actual displacement of the horizontal actuator, and H represents the distance from sensor $D2$ to the center line of the horizontal actuator (600 mm).

δ_l is the relative sliding displacement between the wall and the pedestal, which is the difference between the data recorded by sensors $D3$ and $D4$: $\delta_l = (D_3 - D_4)$.

δ_φ is the displacement of the top of the wall caused by the wall rotation: $\delta_\varphi = \frac{H}{L+B+C} \cdot \delta_a$, $\delta_a = (D_6 - D_8) - (D_5 - D_7)$, where L is the length of the wall, and B and C represent the distances from sensors $D3$ and $D4$ to the top of the lateral side of the wall ($B=C=100$ mm).

The actual shear deformation of the wall is as follows

$$\Delta = \delta = \frac{1}{2}\left(\frac{HD_2}{H-600}+D_1\right) - (D_3 - D_4) -$$
$$\frac{H}{L+B+C}\left[(D_6 - D_8) - (D_5 - D_7)\right] \qquad (2)$$

The hysteretic loops of the horizontal load versus the displacement response for the wall under cyclic loading are presented in Fig. 8 (a)-(f). The skeleton curve for the wall is the envelope formed by connecting all of the peak points of the hysteretic curve (connecting the peak points of the hysteretic curve in the first cycle of the three cyclic groups). The maximum load on the skeleton curve and the corresponding lateral displacement are defined as the peak load, P_{max}, and the corresponding deformation, Δ_{max}, of the wall, respectively. After the peak load is reached, the load on the skeleton curve and the corresponding lateral displacement when the load decreases to 85% of the maximum load is defined as the ultimate load, P_u, and corresponding deformation, Δ_u, of the wall, respectively. The yield load and yield displacement were determined using the area reciprocal method on the skeleton curve according to JGJ 101-2015[12]. The ductility coefficient is the ratio of the peak displacement and yield displacement, i.e., $\mu = \Delta_u/\Delta_y$. The energy dissipation factor, E, is used to measure the energy dissipation capacity of the specimen; the calculation is given in Eq. (3) and Fig. 9.

$$E = \frac{\text{Area of envelope of hysteretic loop } S_{(ABC+CDA)}}{\text{Area of the triangle } S_{(OBE+ODF)}}$$
$$(3)$$

(a) Wall A1-1

(b) Wall A1-2

(c) Wall A2-1

(d) Wall A2-2

(e) Wall A3-1

(f) Wall A3-2
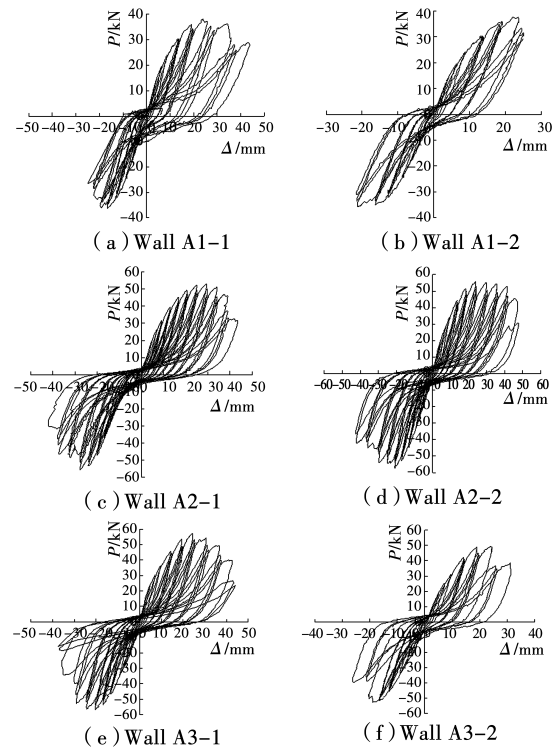
Fig. 8 Hysteresis curve of

3.3 Analysis of the test results

The test data for the six composite walls are summarized in Table 4. From Fig. 8 (a)-(f) and Table 4, the following can be observed:

All six composite walls had similar hysteresis curves. Owing to the improvement in the lateral stiffness of the wall caused by the diagonal bracing
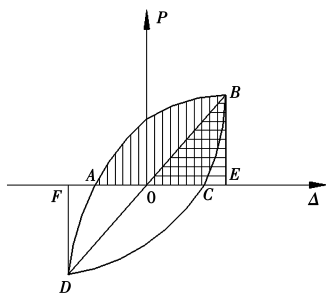
Fig. 9   Calculation method of energy dissipation coefficient

and the gusset plate, the hysteresis curves were full and fusiform at the beginning of the test, and almost no wall slipping occurred. When the horizontal displacement reached a certain degree, the wall entered the plastic stage, the hysteresis curve became arched, the area of the hysteresis loop increased, and the hysteresis curve exhibited a " pinch" phenomenon. At the same horizontal displacement, the area of the hysteresis curve decreased with the increasing number of cycles, and the bearing capacity decreased. In the process

of horizontal pushing and pulling, the wall exhibited some "no-load slipping" behavior. However, the unloading stiffness was relatively large, the curve of the unloading phase had an obvious slope, and the wall had a little restoring force. Thus the residual deformation of unloading was relatively small. As the horizontal displacement continued to increase, the stiffness of the wall gradually decreased, and the hysteresis curve transformed from a bow-shape to an inverse S-shape. At the end of the test, the stiffness degradation of the wall was intensified, the bearing capacity was significantly reduced, the slip of the wall increased, and the horizontal segment of the hysteresis loop became longer. At this time, the energy dissipation capacity of the wall was low, and the "pinching" phenomenon in the middle of the hysteresis loop was more obvious. The energy dissipation capacity of wall A1 was better than that of walls A2 or A3.

Table 4   Data processing results of wall shear test

Wall number	Peak load P_{max}/kN	Peak displacement Δ_{max}/mm	Yield load P_y/kN	Yield displacement Δ_y/mm	Ultimate load P_u/kN	Ultimate displacement Δ_u/mm	Ductility factor μ	Energy dissipation factor E	Shear bearing capacity/ $(kN \cdot m^{-1})$
A1-1	38.23	23.87	32.73	15.66	32.50	35.71	2.28	0.67	15.93
A1-2	37.65	22.11	33.06	15.46	32.00	23.97	1.55	0.64	15.69
A2-1	53.06	23.94	45.78	17.26	45.10	38.67	2.24	0.49	22.11
A2-2	55.72	23.86	49.07	16.54	47.36	44.39	2.68	0.46	23.22
A3-1	57.03	24.46	48.91	15.97	48.48	37.43	2.34	0.51	23.76
A3-2	50.50	22.11	45.63	16.02	42.93	26.62	1.66	0.71	21.04

The shear bearing capacity of wall specimen A2 was 38.79% higher than that of wall specimen A1, but the difference in the ductility coefficient, μ, of the two was not significant, indicating that the restraint effect of the panel on the wall was strong and the shear bearing capacity of the wall was improved markedly. The shear bearing capacity of wall specimen A3 was 7.5% higher than that of wall specimen A2 However, the difference in the ductility coefficient, μ, was not significant, indicating that the shear bearing capacity and ductility coefficient of the wall were

improved by the action of the large axial compression ratio but not significantly.

4   Finite element analysis

4.1   Finite element verification

Finite element (FE) models of the tested composite walls were constructed using the FE software ABAQUS 6.14. S4R shell elements with linear reduced integration were used to simulate the wall skeleton, gusset plate, and OSB panel. The FE model of wall A2 is shown in Fig. 10.

The grid size of the wall steel skeleton and
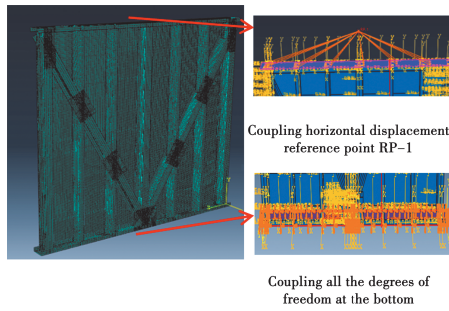
Fig. 10　Finite element model of wall A2

OSB panel was 20 mm，while the grid size of the gusset plate was 10 mm. The following values were used：for the steel，a yield strength $f_y = 358$ MPa，modulus of elasticity $E = 178\ 820$ MPa，and Poisson's ratio $v = 0.3$；for the OSB panel，which was simplified as an isotropic material，a tensile strength $f_u = 7.86$ MPa，modulus of elasticity $E = 3\ 500$ MPa，and Poisson's ratio $v = 0.3$. The self-tapping screw connection was created from the joint section in the interaction module and the translation type of the self-tapping screw connection was defined as a sliding plane. The rotation type was defined such that the U1 of each connection in the local coordinate system （perpendicular to the plane of the panel） was constrained，while U2 （the direction of the vertical actuator） and U3 （the direction of the horizontal actuator） had editable degrees of freedom. Based on shear tests of the self-tapping screw connection，the load-displacement curves for the connection between the OSB panel and steel plate and the steel plate-steel plate were obtained as the parameter options for this connection section[13]. The six degrees of freedom were constrained in the global coordinate system of the web of the bottom beam to simulate the fixed boundary conditions at the bottom of the wall. Reference point RP-1 was established for coupling the connection with the web of the top beam of the wall.

Besides the degrees of freedom in the movement direction of the top beam represented by U2 and U3，the other four degrees of freedom were constrained. Meanwhile，for reference point RP-1，the displacement-loading amplitude was set to be the same as the displacement of the hysteretic loading to simulate the loading process of the tests.

A comparison between the hysteresis curve obtained with the FE analysis and the hysteresis curve obtained in the experiments is shown in Fig. 11. A similar comparison of the skeleton curves is shown in Fig. 12，and comparisons of the FE and experimental yield load，peak load，and shear bearing capacity is given in Table 5.

Fig. 11，12，and Table 5 indicate that the hysteresis curve and skeleton curve obtained with the FE analysis were roughly consistent with the experimental curves. However，the hysteresis loop from the FE results is fuller than that from the experimental results.

Table 5　Comparison between the average of the experimental results and the finite element analysis results

Model		Yield load P_y/kN	Yield displacement Δ_y/mm	Peak load P_{max}/kN	Peak displacement Δ_{max}/mm	Shear bearing capacity/(kN·m^{-1})
Wall A1	Test	32.90	15.56	37.94	29.84	15.81
	Finite element	35.14	14.25	39.61	20.91	16.50
	Error/%	6.81	8.42	4.40	30.00	4.36
Wall A2	Test	47.43	16.90	54.39	23.90	22.67
	Finite element	54.07	15.97	60.90	21.73	25.38
	Error/%	14.0	5.5	12.0	9.08	11.95
Wall A3	Test	47.27	16.0	53.77	23.29	22.40
	Finite element	54.22	15.71	61.22	21.66	25.51
	Error/%	14.70	1.81	13.86	7.0	13.88

The error of the yield load and yield displacement, peak load and peak displacement, and shear bearing capacity of the wall between the FE analysis and the experimental results was generally less than 15%, which indicates that the FE model can effectively simulate the mechanical performance of the wall under hysteresis loading, and the finite element model is reliable.

（a）Comparison of wall A1-1

（b）Comparison of wall A2-1

（c）Comparison of wall A3-1
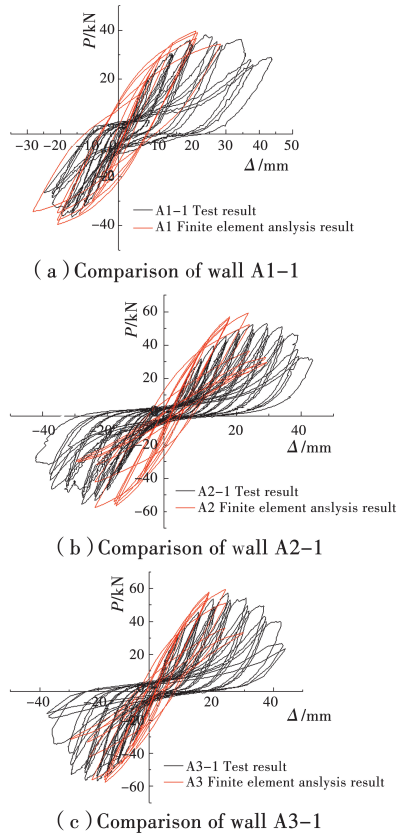
Fig. 11   Comparison of the hysteresis curve between the finite element and test

4.2   Influence of the yield strength of steel on the seismic performance of the wall

Based on the FE model of the cold-formed thin-walled steel composite wall with a single-sided OSB panel and diagonal bracing （wall A2）, the influence of steel strength grades Q235 （$f_y = 245$ N/mm²） and Q345 （$f_y = 358$ N/mm²） on the mechanical properties of the wall was investigated. The FE modeling method was the same as in Section 4.1, and the vertical load was 80 kN. Comparisons of the obtained hysteresis curves and skeleton curves are shown in Fig. 13.

（a）Comparison of wall A1

（b）Comparison of wall A2

（c）Comparison of wall A3
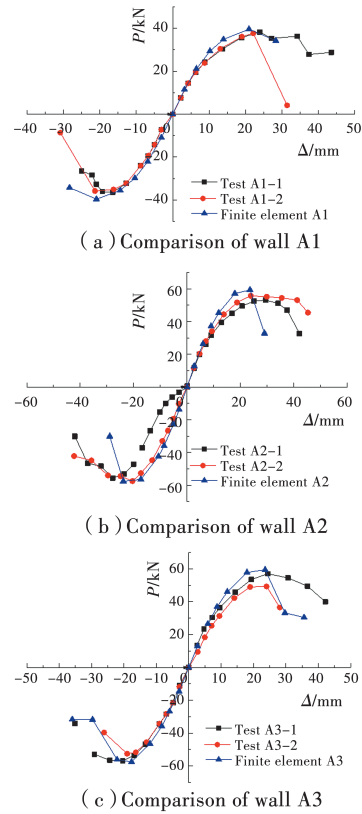
Fig. 12   Comparison of the skeleton curve between the finite element and test

As shown in Fig. 13, compared with the Q235 steel wall, the yield load of the Q345 steel wall was increased by 39.68%, the yield displacement was increased by 37.08%, the peak load was increased by 38.25%, the peak displacement was increased by 25.61%, and the shear bearing capacity was increased by 35.31%. The shear bearing capacity of the composite wall was thus significantly improved by increasing the yield strength of the steel skeleton. This is because the failure of the wall was mainly caused by the yielding of the studs and guide rails, the yielding or fracture of the diagonal bracing at the area of the gusset plate during the process of tension and compression, the shear failure of the screws at the area of joint plate and the corner of the wall plate, and the shear failure of the wall panel. Therefore, the yield strength of the steel is an important factor affecting the shear bearing capacity of walls with diagonal bracing.

(a) Hysteretic curve
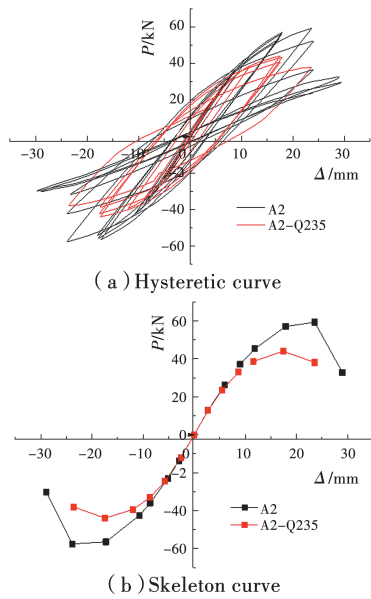
(b) Skeleton curve

Fig. 13   The hysteresis and skeleton curves of finite element analysis

4.3   Influence of the vertical load on the seismic performance of the wall

Based on the FE model of the cold-formed thin-walled steel composite wall with a single-sided OSB panel and diagonal bracing (wall A2), the influence of varying the vertical load (0, 80, 120, 160, 200, 240, 280, and 320 kN) on the mechanical properties of the wall was investigated. The FE modeling method was the same as in Section 4.1. The specimen numbering scheme is summarized in Table 6. A comparison of the skeleton curves for the eight models is shown in Fig. 14. The relationship between the peak load and the axial compression ratio of the wall is shown in Fig. 15, and the results of the FE analysis of the wall specimens are presented in Table 6.

Table 6   The finite element analysis results of the walls

Model number	Vertical load /kN	Axial compression ratio	Yield load P_y/kN	Yield displacement Δ_y/mm	Peak load P_{max}/kN	Shear bearing capacity /(kN·m^{-1})
A2-0	0	0	53.30	16.68	59.43	24.76
A2-80	80	0.16	54.07	15.97	60.90	25.38
A2-120	120	0.24	54.22	15.71	61.22	25.51
A2-160	160	0.32	54.79	15.66	61.96	25.82
A2-200	200	0.40	54.90	15.61	62.32	25.97
A2-240	240	0.48	55.67	15.59	62.82	26.18
A2-280	280	0.56	55.92	15.57	62.91	26.21
A2-320	320	0.64	56.02	15.56	62.94	26.23
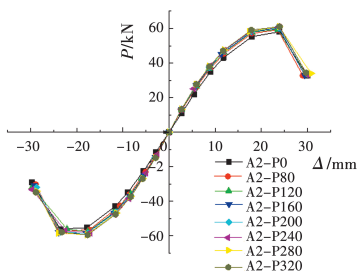
Fig. 14   The comparison of skeleton curves

Fig. 15   The relationship between peak load and axial compression ratio

As indicated in Table 6, Fig. 14, and Fig. 15, the load-displacement curves of the walls under a vertical load exhibited roughly the same trend, and there was little variation in the peak load. With the increasing axial compression ratio, the peak load of the wall gradually increased, and the content of this increase varied from high to low. When the axial compression ratio reached approximately 0.6,

the peak load of the wall tended to be stable. The yield displacement of the wall increased with the increasing axial compression ratio，which indicates that the lateral stiffness of the wall also increased with the increasing vertical load.

For the ordinary steel plate shear wall，the steel plate was confined only by the steel frame and the middle area of the steel plate was unconstrained. The vertical load would lead to the increase of the out-of-plane deformation of the steel plate shear wall，and the reduction of lateral stiffness and shear bearing capacity[5]. But for the cold-formed thin-walled steel composite wall，the application of a vertical load was likely to strengthen the constraint effect of the panel on the steel skeleton. The shear bearing capacity under a vertical load of 320 kN（axial compression ratio of 0.64）was 5.9% higher than that under no vertical load. The increase was not obvious，and the specific reasons need to be studied in further research.

In conclusion，the application of a vertical load was likely to strengthen the constraint effect of the panel on the steel skeleton. The bearing capacity and lateral stiffness of the wall both slightly increased with the increasing axial compression ratio. When the axial compression ratio reached approximately 0.6，the peak load of the wall tended to be stable.

5　Design suggestions for cold-formed thin-walled steel composite walls with diagonal bracing

Based on the safety factor for the allowable stress design in American code AISI-15[14]，the "equal safety factor" principle is used to approximate the "equivalent resistance partial factor" according to the probability limit-state design method in China. This is then combined with the yield bearing capacity to obtain the design value for the shear bearing capacity of composite walls. This method ensures that the calculation

results are basically the same as the reliability in the American code.

Allowable stress design（ASD）for horizontal earthquake action can be described as follows

$$S_{Ehk} \leqslant \frac{P_{nominal}}{K} \qquad (4)$$

where S_{Ehk} is the standard value of the horizontal shear force of the wall under horizontal earthquake action；$P_{nominal}$ is the "nominal shear strength" of the wall，which is taken as the unit peak load of the wall，P_{max}；and K is the safety factor，which is defined as 2.5 under horizontal earthquake action.

The expression for the probability limit state design method in China for horizontal earthquake action is as follows

$$\gamma_0 \gamma_{Eh} S_{Ehk} \leqslant \frac{P_k}{\gamma_R} \Rightarrow S_{Ehk} \leqslant \frac{P_k}{\gamma_0 \gamma_{Eh} \gamma_R}, \qquad (5)$$

where，γ_0 is the coefficient for the importance of a structure，which is generally taken as 1.0；γ_{Eh} is the partial factor of the horizontal earthquake action，taken as 1.3；P_k is the standard value of the shear bearing capacity of the wall，taken as the unit yield load of the wall，P_y[11]；and γ_R is the partial factor for the resistance of the wall.

The monomials on the right sides of Eqs.（4）and（5）were equated and simplified to obtain the partial factor for the resistance of the wall under the action of a horizontal earthquake.

$$\gamma_R = \frac{K P_k}{\gamma_0 \gamma_{Eh} P_{nominal}} = \frac{2.5 P_y}{1.3 P_{max}}. \qquad (6)$$

At present，structural design in China employs the probability limit state design method. The determination of the design value for the shear bearing capacity of the wall，P，mainly involves the standard value of the shear bearing capacity，P_k，and the resistance partial factor，γ_R，of the structure，as follows[15]

$$P = \frac{P_k}{\gamma_R}. \qquad (7)$$

By substituting Eq.（6）into Eq.（7），the design value for the shear bearing capacity of the wall under horizontal earthquake action can be obtained as follows

$$P = 0.52P_{\max} \tag{8}$$

According to the above method, the recommended design values for the shear bearing capacity per unit length of the composite walls obtained through the experiments and FE analysis are listed in Table 7.

Table 7   Shear capacity design values under horizontal earthquake action

Wall number	Wall parameters	Steel strength /kN	Vertical load /kN	Axial compression ratio	Unit peak load/ $(kN \cdot m^{-1})$	Unit yield load/ $(kN \cdot m^{-1})$	Resistance partial factor	Design value of shear bearing capacity/$(kN \cdot m^{-1})$	
A1-1	2.4 m×2.4 m	Q345	80	0.16	15.93	13.64	1.65	8.27	Test
A1-2	No panel		80	0.16	15.69	13.78	1.69	8.15	
A2-1	2.4 m×2.4 m		80	0.16	22.11	19.08	1.66	11.49	
A2-2	single-sided		80	0.16	23.22	20.45	1.69	12.10	
A3-1	OSB panel		120	0.24	23.76	20.38	1.65	12.35	
A3-2			120	0.24	21.04	19.01	1.74	10.93	
A1	2.4 m×2.4 m No panel	Q345	80	0.16	16.50	14.64	1.71	8.56	Finte element
A2(A2-80)			80	0.16	25.38	22.53	1.71	13.18	
A3(A2-120)			120	0.24	25.51	22.59	1.70	13.29	
A2-0			0	0.00	24.76	22.21	1.73	12.84	
A2-160	2.4 m×2.4 m		160	0.32	25.82	22.83	1.70	13.43	
A2-200	single-sided		200	0.40	25.97	22.88	1.69	13.54	
A2-240	OSB panel		240	0.48	26.18	23.20	1.70	13.65	
A2-280			280	0.56	26.21	23.30	1.71	13.63	
A2-320			320	0.64	26.23	23.34	1.71	13.65	
A2-Q235		Q235	80	0.16	18.35	16.13	1.69	9.54	

Based on the results in Table 7, test behavior observations, and the wall structure and influencing factors for the shear bearing capacity of the wall, the following design suggestions for cold-formed thin-walled steel composite walls with diagonal bracing are proposed:

1) In the tests, the failure of the composite wall with a single-sided OSB panel mostly occurred in the gusset plate area and the corner of the panel. This was shown by the shear fracture of the screws in the gusset plate area, the breakage of the diagonal bracing caused by the reciprocating deformation of the flange in the process of tension and compression, the yielding of the studs and the lower guide rail, and the shear fracture at the corner of the panel. Finally, shear fracture of the screws on the gusset plate represented the failure

of the wall. Therefore, it is recommended to include a gusset plate at the intersection of the diagonal bracing and the steel skeleton in the design of these walls.

2) The yield strength of steel is an important factor affecting the shear bearing capacity of walls with diagonal bracing. Thus, it is suggested that in the design of cold-formed thin-walled composite walls with diagonal bracing, steel with a higher yield strength should be selected.

3) For the cold-formed thin-walled steel composite wall, the application of a vertical load was likely to strengthen the constraint effect of the panel on the steel skeleton, and the shear bearing capacity under a vertical load of 320 kN (axial compression ratio of 0.64) was 5.9% higher than that under no vertical load. But the increase was

not obvious，therefore，it is suggested that the influence of the vertical load on the shear bearing capacity of the wall should not be the focus of too much attention in the design of cold-formed thin-walled steel composite walls with diagonal bracing.

6   Conclusions

In this study，through an experimental investigation and FE analysis of the seismic performance of diagonally braced cold-formed thin-walled steel composite walls subjected to a vertical load，the following conclusions could be drawn：

1）The failure of walls with no panel mostly occurred in the joint area. This manifested as inclined slippage and shear fracture of the screws in the gusset plate area，breakage of the diagonal bracing caused by the reciprocating deformation of the flange in the process of tension and compression，and yielding of the flange of the lower guide rail and the bottom of the middle studs. The failure mode observed in the composite wall with a single-sided OSB panel was mostly oblique slipping and shear fracture of the screws in the gusset plate area，severe deformation and yielding of the studs and the lower guide rail，and shear fracture of the screws at the corner of the panel and the joint area. The studs in composite walls with a higher axial pressure yielded earlier and exhibited more deformation when destroyed.

2）The panel had a strong restraint effect on the composite wall and made a significant contribution to improving the shear bearing capacity of the diagonally braced wall. The yield strength of the steel was an important factor affecting the shear bearing capacity of walls with diagonal bracing. However，the axial compression ratio had little influence on the shear bearing capacity of the wall，and when the axial compression ratio reached a certain level，the shear bearing capacity fluctuated minimally and became stable.

3）Based on the experiments and FE analysis and according to the design norms and theoretical background of JGJ 227-2011 and American code AISI-15，"the partial coefficient of resistance" of the wall was derived，and the design value for the shear bearing capacity of the wall under the action of a horizontal earthquake was determined，providing a reference to guide the structural design of these walls.

Acknowledgements

References：

［1］ BLUM H B，MEIMAND V Z，SCHAFER B W. Flexural bracing requirements in axially loaded cold-formed steel-framed walls［J］. Practice Periodical on Structural Design and Construction，2015，20（4）：04014043.

［2］ HIKITA K，ROGERS C A. Impact of gravity loads on the lateral performance of light gauge steel frame/wood panel shear walls ［C］//Ninth Canadian Conference on Earthquake Engineering，Ottawa，Ontario，Canada，2007.

［3］ TIAN Y S，WANG J，LU T J. Racking strength and stiffness of cold-formed steel wall frames［J］. Journal of Constructional Steel Research，2004，60（7）：1069-1093.

［4］ GAD E F，DUFFIELD C F，HUTCHINSON G L，et al. Lateral performance of cold-formed steel-framed domestic structures［J］. Engineering Structures，1999，21(1)：83-95.

［5］ LIU K Z. Hysteretic behavior of steel plate shear walls and buckling-restrained steel plate shear walls

considering vertical load［D］. Harbin：Harbin Institute of Technology，2015.

［6］ HAO J P，LIU B，SHAO D Y，et al. Test on shear resistance of cold-formed thin-walled X-shaped steel strap-braced framing walls with sprayed lightweight mortar［J］. Journal of Building Structures，2014，12 (35)：20-28.

［7］ DONG H T. Research on the shear resistance of sandwich plate cold-formed steel composite wall［D］. Xi'an：Chang'an University，2011.

［8］ CHEN W H. Study on shear performance of high strength cold-formed steel framing walls with cross bracing［D］. Xi'an：Xi'an University of Architecture and Technology，2008.

［9］ WANG Y H，DENG R，YAO X M，et al. Experiment on seismic behaviour of cold-formed thin-walled steel walls with diagonal braces［J］. Journal of Architecture and Civil Engineering，2019，36(2)：34-42.

［10］ Metallic materials-tensile testing-Part I：Method of at room temperature：GB/T 228. 1-2010［S］. Beijing：Standard Press of China，2010.

［11］ Technical specification for low-rise cold-formed thin-walled steel buildings：JGJ 227-2011［S］. Beijing：China Architecture and Building Press，2011.

［12］ Specification for seismic test of buildings：JGJ 101-2015［S］. Beijing：China Architecture and Building Press，2015.

［13］ XIA X. Seismic performance of the cold-formed thin-walled steel composite wall with diagonal bracing and vertical load ［D］. Chongqing：Chongqing University，2018.

［14］ North American Standard for Seismic Design of Cold-Formed Steel Structural Systems：AISI S400-15［S］. Washington，DC：American Iron and Steel Institute，2001.

［15］ Load code for the design of building structures：GB 50009-2012［S］. Beijing：China Architecture and Building Press，2012.

（编辑　章润红）